Available online at www.sciencedirect.com
ScienceDirect
Journal of Sound and Vibration 307 (2007) 20–37
JOURNAL OF SOUND AND VIBRATION
www.elsevier.com/locate/jsvi

Optimal probabilistic design of the dynamic performance of a vibration absorber

Young Kap Son, Gordon J. Savage*

Systems Design Engineering, University of Waterloo, Waterloo, Ontario, Canada N2L 3G1

Received 16 November 2005; received in revised form 18 September 2006; accepted 7 June 2007

Abstract

This paper presents a non-sample-based probabilistic approach to determine the parameters in a vibration absorber when the main system is described by random variables. The sinusoidal steady-state amplitude of the main mass is considered as the dynamic performance measure. The design goal is to reduce both the mean and variance of the dynamic performance measure over the excitation frequency range. The design process is complicated because the resonance frequency of the main system is also a random variable. In order to address these difficulties, system-specified, maximum, critical amplitudes according to three critical frequencies capable of representing the excitation frequency range are established. Then limit-state functions are formed at each of the critical frequencies by subtracting the respective dynamic performance measure from the critical amplitude. Each limit-state function establishes a non-conformance region in terms of the random variables. The probability of the union of the non-conformance regions provides a single objective to be minimized by adjusting the design parameters in the vibration absorber. A first-order reliability method is implemented to efficiently estimate probabilities. Monte-Carlo sampling is invoked to verify our method. The proposed approach for the absorber design is compared with a deterministic approach and a second-order transmission of moments approach available in the open literature. The proposed approach is found to be robust, expandable and flexible.

1. Introduction

Many engineering systems fail due to vibration. For example, in microelectronics, vibration is the second highest cause of failures, which accounts for 27% of the total failures (failures due to temperature are predominant at about 40%). The vibration of electronic systems manifests itself in several ways: connections fail, or indeed, components may break off the circuit board. In mechanical systems, excessive vibration levels induce, for example, structural safety problems (e.g. fatigue) as well as human discomfort (e.g. motion sickness). Deterministic optimization has produced greatly improved performance in all types of engineering systems. It can however, lead to unreliable design if the uncertainty is ignored.

All systems exhibit uncertainty. This arises from (a) input uncertainty (e.g. loadings, supply voltages, etc.), and (b) component variation (e.g. resistance and dimensional tolerances, etc.) that results in performance (e.g.

*Corresponding author. Tel.: +1 519 888 4567x3941; fax: +1 519 746 4791.
E-mail address: gjsavage@uwaterloo.ca (G.J. Savage).

0022-460X/$ - see front matter
doi:10.1016/j.jsv.2007.06.032

responses) variations. Robust design is a methodology that attempts to ensure that the responses are insensitive to both the input uncertainty and component variations without actually eliminating the causes. Specifically, examples of robust design include parameter design wherein means are adjusted while keeping tolerances steady [1], tolerance design where means are kept constant and tolerance are adjusted to reach a minimum cost [2,3], integrated design where means and tolerance are adjusted simultaneously [4–6], and conformance-based design where the well-known Design for Six Sigma [7] is an example. Robust design has been applied to a wide variety of static performance-related problems. There have been a few applications of robust design to dynamic performance with respect to the reduction of vibration levels in mechanical systems. Seki et al. [8] applied the robust design concept to the dynamic design of an optical pick-up actuator focusing on shape synthesis of a leaf spring using mechanistic performance models and design of experiments. The thickness and the modulus of elasticity of the leaf spring were considered to be the design variables. The natural frequency of the actuator, and the response gain at the natural frequency were selected as the two performance measures. The "nominal-is-best" signal-to-noise ratio served as the quality metric for the natural frequency, and the "smaller-is-better" signal-to-ratio served as the quality metric for the response gain. The optimal width was determined by minimizing simultaneously the mean and variance of the performance measures. In another paper, Hwang et al. [9] minimized mean and standard deviation of the displacement at the first resonance frequency of an automobile mirror system with both stiffness and mass variation using Taguchi's smaller-is-better loss function. Finally, of direct relation to this paper, Zang et al. [10] applied robust design to the two-degree-of-freedom (2-dof) system shown in Fig. 1.

They considered the main mass (m_1) and stiffness (k_1) to be uncertain and assigned normal probability distributions. They let the performance measure be the normalized amplitude of the main mass, denoted herein as A_n. Then they derived its mean $\mu(A_n)$ and variance $\sigma^2(A_n)$ using first-order Taylor series approximations comprising means and variances of m_1 and k_1. Next, they produced a single objective in the form

$$G = \alpha \frac{\mu(A_n)}{\mu^*(A_n)} + (1-\alpha)\frac{\sigma(A_n)}{\sigma^*(A_n)}, \tag{1}$$

where μ^* and σ^* are the best-case design values and α is a weight that spans from zero to one. Finally, they simplified the analysis by setting the excitation frequency to be the natural frequency of the main system. In order to help determine the three parameters in the absorber subsystem, (i.e. m_2, k_2 and c_2), they applied optimization to minimize G. Various designs were obtained for a range of weightings given by α. For the most robust design they subjectively selected the design that appeared to simultaneously minimize $\mu(A_n)$ and $\sigma(A_n)$. Their approach increased robustness when compared to deterministic designs in Refs. [11,12].

In this paper a new, non-subjective, probabilistic approach is proposed to determine the stiffness, mass and damping parameters of a vibration absorber when there is uncertainty in the main mass and stiffness. The approach ensures that the amplitude of the main mass is within a critical limit over a wide range of excitation frequencies. In Section 2, the vibration absorber system to be designed and its mechanistic model in terms of

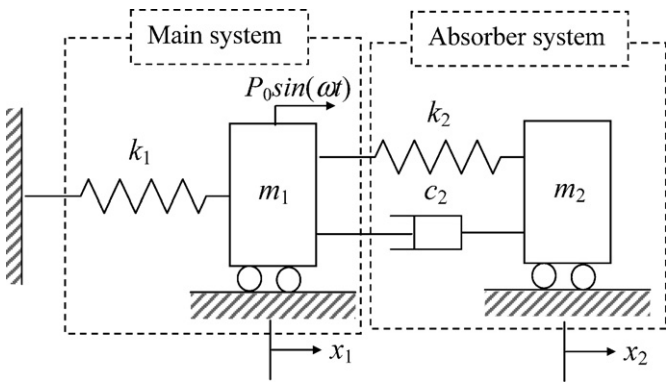

Fig. 1. Two-degree-of-freedom system comprising the main system and an attached damped vibration absorber.

dynamic performance are introduced. Next, a deterministic optimization problem is formulated to minimize the amplitude of the main mass at three critical frequencies simultaneously. Then, the formulation is extended to include the probabilistic nature of the problem. In Section 3, limit-state functions and first-order reliability methods (FORM) for probability evaluations are introduced. An optimization problem that addresses robustness is developed in terms of the combined probability of non-conformance at the critical frequencies. In Section 4, the design approach is applied to design a vibration absorber of a footbridge. Comparisons with other previous approaches are discussed. Section 5 shows advanced analyses.

2. Vibration absorber modeling and design approaches

2.1. Response modeling

As shown in Fig. 1, the main system is excited by a sinusoidal force of constant amplitude P_0 with a wide range of excitation frequencies (ω). An approach to protecting the main system from steady-state disturbances at the resonance frequency of the main system (without the absorber system) is to use a vibration absorber. From [12], resonance frequency of the main system (1-dof system) without the absorber system has a form

$$(\omega)_{1-\mathrm{dof}} = \sqrt{\frac{k_1}{m_1}}. \tag{2}$$

When the absorber system is attached to the main mass (m_1), the main system has changed from a 1-dof system to a 2-dof system (the main system attached with the absorber system). For the 2-dof system, the equations of motion in terms of displacements of the two masses from their at-rest-positions are [10–12]:

$$\begin{aligned} &m_1\ddot{x}_1 + c_2(\dot{x}_1 - \dot{x}_2) + k_1x_1 + k_2(x_1 - x_2) = P_0\,\sin(\omega t),\\ &m_2\ddot{x}_2 + c_2(\dot{x}_2 - \dot{x}_1) + k_2(x_2 - x_1) = 0. \end{aligned} \tag{3}$$

The complete solutions to the two-coupled equations in Eq. (3) comprise both a transient and a steady-state part. Herein the transient responses are considered negligible and thus only the (sinusoidal) steady-state responses are considered. We let the parameters for the main subsystem be $\mathbf{v} = [m_1,k_1]$ and the design parameters in the vibration absorber be $\mathbf{p} = [m_2,k_2,c_2]$. The two, steady state, amplitudes of the vibrating masses are, respectively [10–12],

$$|x_1| = P_0\left(\frac{c_2^2\omega^2 + (k_2 - m_2\omega^2)^2}{c_2^2\omega^2(k_1 - m_1\omega^2 - m_2\omega^2)^2 + (k_2m_2\omega^2 - (k_1 - m_1\omega^2)(k_2 - m_2\omega^2))^2}\right)^{1/2}, \tag{4}$$

$$|x_2| = P_0\left(\frac{c_2^2\omega^2 + k_2^2}{c_2^2\omega^2(k_1 - m_1\omega^2 - m_2\omega^2)^2 + (k_2m_2\omega^2 - (k_1 - m_1\omega^2)(k_2 - m_2\omega^2))^2}\right)^{1/2}. \tag{5}$$

In order to provide comparisons with work in Refs. [10–12], we define $x_{\mathrm{static}} = P_0/k_1$ to be the static deflection of the main mass. Now, the *normalized* amplitude of interest, obtained by dividing Eq. (4) by the static deflection, is

$$a_n(\mathbf{p},\mathbf{v},\omega) = k_1\left(\frac{c_2^2\omega^2 + (k_2 - m_2\omega^2)^2}{c_2^2\omega^2(k_1 - m_1\omega^2 - m_2\omega^2)^2 + (k_2m_2\omega^2 - (k_1 - m_1\omega^2)(k_2 - m_2\omega^2))^2}\right)^{1/2}. \tag{6}$$

For no damping ($c_2 = 0$), the 2-dof system has two resonance frequencies, neither of which equals the original resonance frequency of the main mass (and also the absorber). The two resonance frequencies of the 2-dof system has forms:

$$(\omega_1)_{2\text{-dof}} = \left(\left(\frac{k_1}{2m_1}\right)\left(1 + q^2(1+\eta) - (q^4(1+\eta)^2 - 2(1-\eta)q^2 + 1)^{1/2}\right)\right)^{1/2}, \tag{7}$$

$$(\omega_2)_{2\text{-dof}} = \left(\left(\frac{k_1}{2m_1}\right)\left(1+q^2(1+\eta)+(q^4(1+\eta)^2-2(1-\eta)q^2+1)^{1/2}\right)\right)^{1/2}. \quad (8)$$

where $q = \sqrt{k_2/m_2}\Big/\sqrt{k_1/m_1}$, and $\eta = m_2/m_1$.

The normalized amplitude of the main mass in the 2-dof system is infinite at these two resonance frequencies. While this may not be a problem when the main mass is running at $(\omega)_{1\text{-dof}}$: (a) the main mass's running at the other frequencies (e.g. during startup and shutdown), (b) a wide range of excitation frequency (ω) including $(\omega_1)_{2\text{-dof}}$ and $(\omega_2)_{2\text{-dof}}$, and (c) variation in $(\omega)_{1\text{-dof}}$ due to manufacturing processes of the main mass (m_1) and stiffness (k_1) could cause an infinite normalized amplitude of the main mass. In practice, a finite amount of damping in the absorber system is used to control the vibration of the main system over a wide frequency range. However if damping is present in the absorber system, the normalized amplitude of the main mass will no longer be zero at $(\omega)_{1\text{-dof}}$. Thus, amplitude of the mass (m_1) in 2-dof system at (a) the resonance frequency of primary system ($(\omega)_{1\text{-dof}}$), (b) two resonance frequencies of the 2-dof system ($(\omega_1)_{2\text{-dof}}$ and $(\omega_2)_{2\text{-dof}}$) could characterize performance of absorber system although the 2-dof system is affected by a wide range of excitation frequency. For notation convenience, we set $w_1 = (\omega_1)_{2\text{-dof}}$, $w_2 = (\omega)_{1\text{-dof}}$, and $w_3 = (\omega_2)_{2\text{-dof}}$ hereinafter.

The significance of $\omega = w_1$, w_2, and w_3 on a_n is shown by an example. Consider a system with $m_1 = 17{,}500\,\text{kg}$, $k_1 = 3\,\text{M N/m}$, $m_2 = 175\,\text{kg}$, and $k_2 = 30\text{k N/m}$ and arbitrary c_2. The resonance frequencies are $w_1 = 12.5\,\text{rad/s}$, $w_2 = 13.1$ and $w_3 = 13.8$ and. Fig. 2 shows the normalized amplitude $a_n(c_2,\omega)$ of the main mass for selected c_2 over the frequency range.

As expected, for $c_2 = 0\,\text{N s/m}$, the maximum amplitudes occur at frequencies w_1 and w_3: there is negligible amplitude at w_2. For ideally large damping (e.g. $c_2 = 20{,}000\,\text{N s/m}$ to show infinite damping value), the maximum amplitude occurs near w_2. Finally, a finite amount of damping (e.g. $c_2 = 272\,\text{N s/m}$) provides for a finite normalized amplitude over the wide range of excitation frequencies, although local maximum and minimum occur near w_1, w_2 and w_3. Ideally, we would like to have the normalized amplitude uniformly small over the entire range of frequencies. Fortunately, as suggested in Fig. 2 and shown more clearly in Fig. 3, a reasonable alternative is to control the normalized amplitudes near the frequencies w_1, w_2 and w_3. Thus, for expediency, we select these three frequencies as critical frequencies to represent the frequency range.

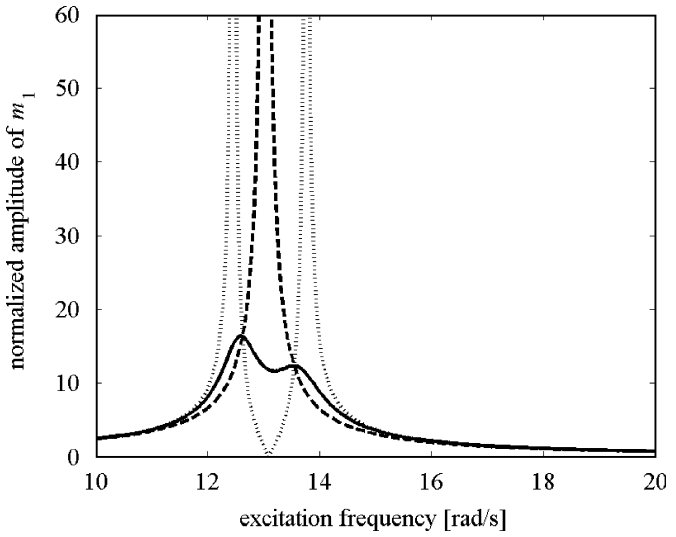

Fig. 2. Normalized amplitude of mass m_1 for three selected damping parameter values: $c_2 = 0$ (dotted line), $c_2 = 272$ (line), and $c_2 = 20{,}000$ (dashed line).

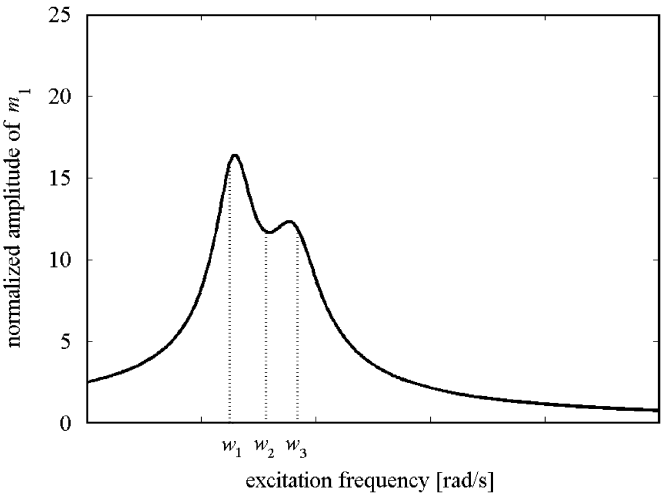

Fig. 3. Normalized amplitude of mass m_1 over frequency range with three critical frequencies emphasized.

2.2. Optimal deterministic design

For now, let the main mass m_1 and stiffness k_1 be fixed and deterministic so $\mathbf{v} = \mathbf{v}_0$. Let us substitute, in turn, $\omega = w_1$, w_2 and w_3 into a_n. Then three distinct corresponding normalized amplitudes arise

$$a_i = a_n(\mathbf{p}, w_i), \quad i = 1, 2, 3. \tag{9}$$

Further, for deterministic components in the absorber system, the critical frequencies w_1, w_2 and w_3 are deterministic, and as is clear in Eqs. (2), (7) and (8) are explicit functions of m_1, k_1, m_2 and k_2. When w_1, w_2 and w_3 are substituted, in turn, into Eq. (9) we get three deterministic performance measures

$$a_i = z_i(\mathbf{p}), \quad i = 1, 2, 3. \tag{10}$$

In order to control the three normalized amplitudes, we allocate $\mathbf{p}$ through the unconstrained optimization problem

$$\underset{\mathbf{p}}{\text{Minimize}} \quad \sqrt{a_1^2 + a_2^2 + a_3^2}.$$

For example, with $\mathbf{v}_0 = [17{,}500\,\text{kg},\ 3.0\,\text{M N/m}]$ and a given mass ratio $\eta = 1\%$, we find $[m_2,k_2,c_2] = [175\,\text{kg},\ 29{,}577\,\text{N/m},\ 271.1\,\text{N s/m}\ ]$. If we wish to balance the amplitudes at w_1 and w_3, we introduce the constraint $a_1 - a_3 = 0$, and now obtain the deterministic design $\mathbf{p}_D = [m_2,k_2,c_2] = [175\,\text{kg},\ 29{,}393\,\text{N/m},\ 272.2\,\text{N s/m}]$. This result agrees with Refs. [11,12]. The frequency response of $a_n(\mathbf{p}_D,\mathbf{v}_0,\omega)$ is shown in Fig. 4.

2.3. Uncertainty considerations

We now introduce the shortcomings of using a deterministic design when m_1 and k_1 are random variables denoted as V_1 and V_2, respectively. For simplicity in presentation let V_1 and V_2 be lognormally distributed. For the main mass, let $\mu(V_1) = 17{,}500\,\text{kg}$ and $\sigma(V_1) = 10\mu(V_1)/300$. For the stiffness, let $\mu(V_2) = 3.0\,\text{M N/m}$ and $\sigma(V_2) = 10\mu(V_2)/300$. Let us see the shortcomings of the deterministic design $\mathbf{p}_D$ for this situation. We select samples of V_1 and V_2 from their lognormal distributions using random sampling to provide mass and stiffness pairs $[\mathbf{v}_{\#1}],[\mathbf{v}_{\#2}],\ldots,[\mathbf{v}_{\#N}]$ and then substitute them into Eq. (6) to obtain $a_n(\mathbf{p}_D,\mathbf{v}_{\#i},\omega)$. For $N = 5000$ samples, both the maximum and minimum normalized amplitude at each frequency are shown in Fig. 4. In order to place the maximum and minimum in perspective, the normalized amplitude of the deterministic design is shown as well. Indeed the large values of the maximum when there are variations in the mass and stiffness of the main system emphasize the weakness of the absorber design $\mathbf{p}_D$.

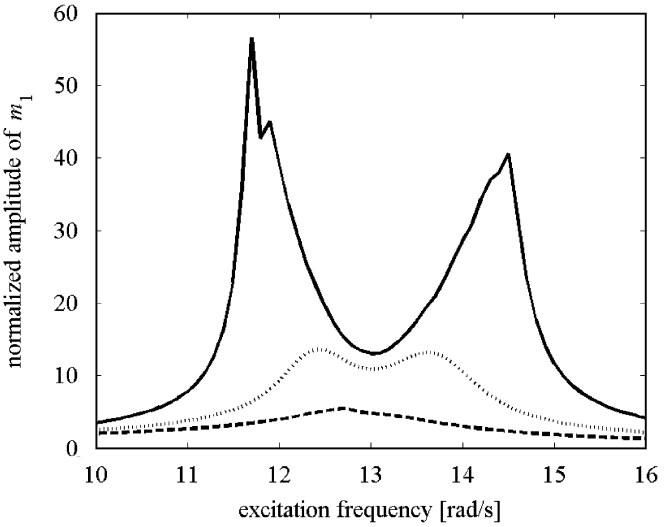

Fig. 4. Normalized amplitude of main mass at each frequency for deterministic design $\mathbf{p}_D$ with m_1 and k_1 lognormally distributed: the dotted line is obtained with $\mathbf{v}_0$ and the line and dashed line represent the maximum and minimum amplitudes, respectively.

One way to measure and then improve the design proceeds as follows. We introduced a maximum normalized amplitude of the main mass, say z_0. In general, this value may be set according to safety and/or comfort considerations. Then for a large sample size N we count the number of systems that have $a_n(\mathbf{p}_D,\mathbf{v}_{\#i},(1<\omega<3w_2)>z_0$, say B, and write the probability of failure as $P(F)=B/N$. A methodology that searches for absorber parameters that reduces $P(F)$, and by definition increases robustness, is needed. This is discussed next.

2.4. Optimal probabilistic design

The deterministic optimization approach and the uncertainty issues developed above guide the way to the formulation of a non-sample based probabilistic approach for finding $\mathbf{p}$ for uncertain main mass (m_1) and stiffness (k_1). Let us emphasize the random nature of m_1 and k_1 by writing them in terms of arbitrary distributions V_1 and V_2, respectively, so $\mathbf{V}=[V_1,V_2]$. Now the normalized amplitude, from Eq. (6), is a random variable

$$A_n(\mathbf{p},\mathbf{V},\omega)=V_2\left(\frac{c_2^2\omega^2+(k_2-m_2\omega^2)^2}{c_2^2\omega^2(V_2-V_1\omega^2-m_2\omega^2)^2+(k_2m_2\omega^2-(V_2-V_1\omega^2)(k_2-m_2\omega^2))^2}\right)^{1/2}. \tag{11}$$

Further, from Eqs. (2), (7) and (8) the critical frequencies are also random variables and are now denoted as W_1, W_2 and W_3. For example, from Eq. (2), the critical frequency w_2 becomes the random variable

$$W_2=\sqrt{V_2/V_1}. \tag{12}$$

More specifically, suppose the mass and stiffness are lognormally distributed, independent. Now we set $\mu(V_1)=17{,}500\,\mathrm{kg}$ with $\sigma(V_1)=10\mu(V_1)/300$ and $\mu(V_2)=3\,\mathrm{M\,N/m}$ with $\sigma(V_2)=10\mu(V_2)/300$. In Fig. 5 is a histogram of W_2 compiled by random sampling with a sample size of $N=1000$. Similar histograms can be constructed for W_1 and W_3. It is clear that the excitation frequency that causes the maximum amplitude is unknown.

Let us follow the lead of the deterministic formulation above and include the random nature of the three critical frequencies in the normalized amplitude in Eq. (11) and write, for $i=1,2,3$,

$$A_n(\mathbf{p},\mathbf{V},W_i)=V_2\left(\frac{c_2^2W_i^2+(k_2-m_2W_i^2)^2}{c_2^2W_i^2(V_2-V_1W_i^2-m_2W_i^2)^2+(k_2m_2W_i^2-(V_2-V_1W_i^2)(k_2-m_2W_i^2))^2}\right)^{1/2}. \tag{13}$$

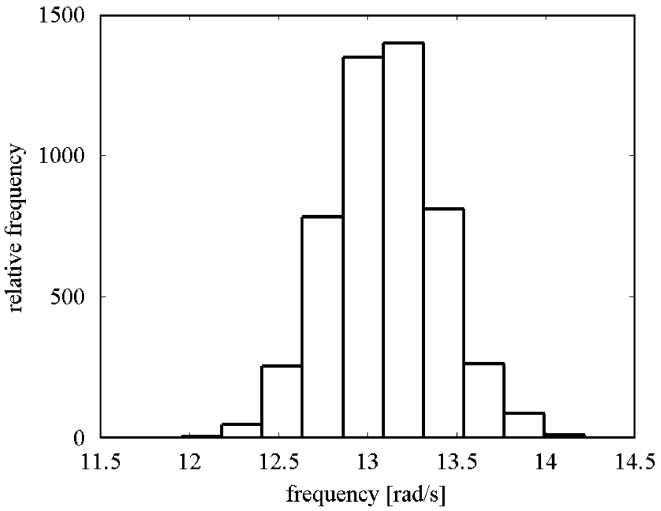

Fig. 5. Histogram of random critical frequency W_2.

When we substitute W_1, W_2 and W_3 (in terms of V_1, V_2, m_2 and k_2) into Eq. (13), in turn, we get the three, random variable, dynamic performance measures of interest

$$Z_i = z_i(\mathbf{p}, \mathbf{V}), \quad i = 1, 2, 3. \tag{14}$$

For example, for Z_2, we have from Eqs. (12) and (13)

$$Z_2(\mathbf{p}, \mathbf{V}) = V_2 \left(\frac{c_2^2\left(\frac{V_2}{V_1}\right) + \left(k_2 - m_2\left(\frac{V_2}{V_1}\right)\right)^2}{c_2^2\left(\frac{V_2}{V_1}\right)\left(V_2 - V_1\left(\frac{V_2}{V_1}\right) - m_2\left(\frac{V_2}{V_1}\right)\right)^2 + \left(k_2 m_2\left(\frac{V_2}{V_1}\right) - \left(V_2 - V_1\left(\frac{V_2}{V_1}\right)\right)\left(k_2 - m_2\left(\frac{V_2}{V_1}\right)\right)\right)^2} \right)^{1/2} \tag{15}$$

and we get similar expressions for Z_1 and Z_3. In order to merge the three performance measures into a single probabilistic measure, we follow the approach used in the design of electrical filters [3]. Therein, critical amplitude limits are specified for a number of critical frequencies according to the filter type and order (e.g. a second-order low-pass filter has three critical limits). For a successful design, all amplitudes must satisfy their corresponding critical limits in a probabilistic sense. In the design of the absorber system, we establish a single critical limit over our range of frequencies that represents the maximum allowable, normalized, amplitude. Then, we find the probability that any of the three performance measures in Eq. (14) exceeds the critical limit. That is, we find

$$P(F) = P((Z_1 > z_0) \cup (Z_2 > z_0) \cup (Z_3 > z_0)). \tag{16}$$

The optimum allocation of m_2, k_2 and c_2 occurs when we minimize $P(F)$. The theory for this approach and its implementation are discussed in detail in the next section.

3. Probabilistic design theory

Consider a system model with q responses $\mathbf{Z}$, written as functions of the m design variables $\mathbf{V}$, in the particular explicit form

$$\mathbf{Z} = z(\mathbf{V}). \tag{17}$$

In general, the design variables $\mathbf{V}$ are random variables with probability distributions. We define a design parameter vector $\mathbf{p} = [p_1, p_2, \ldots, p_{2m}]$, where the parameters p_i and p_{i+m} represent the statistical nature of an arbitrarily distributed design variable V_i. For example, for normal V_i, p_i and p_{i+m} represent the mean and

standard deviation. Most systems have inherent critical operating levels (denoted herein as z_0) such as melting temperatures, over-voltages, or maximum amplitudes. It is then the responsibility of the designer to ensure that the performance measures (e.g. responses) keep within these critical levels. Limit-state functions connect the performance measures to their critical levels, and in terms of samples of the design variables, have the form

$$g(\mathbf{v}) = \pm(z(\mathbf{v}) - z_0), \tag{18}$$

where $z(\mathbf{v})$ is a performance measure and z_0 is either a lower or upper limit specification. (Note: For upper limit specifications the negative of the right side of Eq. (18) is used.) We define, for any limit-state function, three regions:

$g(\mathbf{v}) > 0$, $\mathbf{v} \in$ Conformance region (Success region, S)
$g(\mathbf{v}) = 0$, $\mathbf{v} \in$ Limit-state surface (LSS)
$g(\mathbf{v}) < 0$, $\mathbf{v} \in$ Non-conformance region (Failure region, F).

Examples of these three regions, in terms of two design variables, are shown in Fig. 6.

For m design variables, the LSS has dimension $m-1$. The surface is important since it separates samples of the design variables into those that provide a conforming, or safe design and those that produce a non-conforming, or fail design. Each limit-state function has one non-conforming region, say F_i for the ith limit-state function. Then for n limit-state functions, the union of all such regions defines the system non-conformance region denoted as F. Finally, the set of design variables $\mathbf{V}$ provides a joint probability distribution $f_{\mathbf{V}}(\mathbf{v})$, and when projected over the same space as the limit-state function, the probability of non-conformance for the system is

$$P(F) = P(\cup_{i=1}^{n} F_i) = P(\cup_{i=1}^{n} (g_i(\mathbf{V}) \leqslant 0)) = \iint_F f_{\mathbf{V}}(\mathbf{v})\, \mathrm{d}\mathbf{v}. \tag{19}$$

The system probability of conformance is simply

$$P(S) = 1 - P(F).$$

It is common to estimate the probability integral in Eq. (19) by invoking a hyper-plane approximation to the LSS. In order to see this connection we write, via Taylor series to first order, the conformance margin as the hyper-plane

$$G(\mathbf{V}) \approx g(\mathbf{v}) + [\mathbf{V} - \mathbf{v}]^{\mathrm{T}} \nabla_{\mathbf{V}} g(\mathbf{v}). \tag{20}$$

A particular hyper-plane is formed according to the expansion point in Eq. (20). Most commonly, the point selected comprises the mean values of the design variables. A more rational expansion point is called the most-likely failure point (MLFP) and is the point on the LSS closest to the set of means [13].

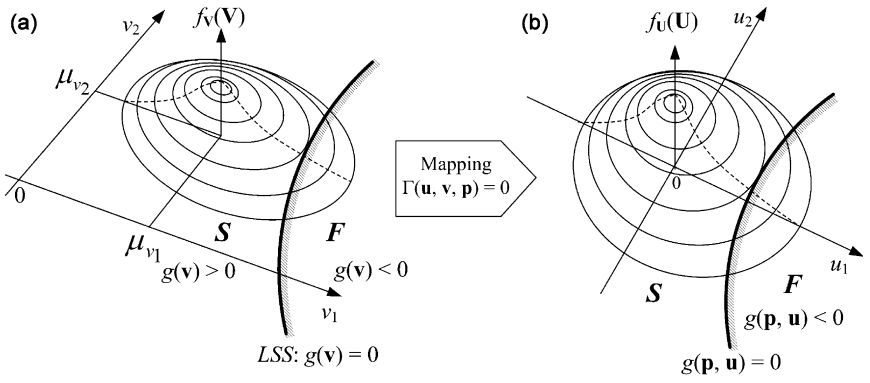

Fig. 6. Limit-state function: (a) $\mathbf{v}$-space, and (b) $\mathbf{u}$-space.

In general, using the Rosenblatt transformation [14], samples of the m arbitrarily distributed design variables (i.e. $\mathbf{v}$) can be mapped to a corresponding vector $\mathbf{u}$ that represents m standard normal variables. By the same transformation, the LSS (and MLFP) in $\mathbf{v}$-space, as shown in Fig. 6(a), may be mapped to $\mathbf{u}$-space (see Fig. 6(b)). The advantage of converting to $\mathbf{u}$-space is that now the probability density has maximum density at the origin and has the same value at all points a constant Euclidean distance away from the origin. The MLFP in $\mathbf{u}$-space, denoted as $(\mathbf{u})^*$, has the highest probability density in the failure region. A hyper-plane approximation to the LSS is obtained by a first-order Taylor expansion of the surface $g(\mathbf{u})$ at $(\mathbf{u})^*$ and in the format of Eq. (20) is expressed as [13]

$$g(\mathbf{p},\mathbf{u}) \approx g(\mathbf{p},\mathbf{u}^*) + (\mathbf{u}-\mathbf{u}^*)^{\mathrm{T}}\nabla_{\mathbf{u}} g(\mathbf{p},\mathbf{u}^*). \tag{21}$$

When Eq. (21) is invoked, we say we are using a FORM. Now, the MLFP satisfies two conditions: first, in order to ensure that the MLFP is on the LSS, we must have $g(\mathbf{p},\mathbf{u}) = 0$. Next, to ensure we have the closest point, we must have the vector $\mathbf{u}^*$ co-linear with the gradient $\nabla_{\mathbf{u}} g(\mathbf{p},\mathbf{u}^*)$. Another more computationally effective way of writing the last condition is to use the actual hyper-plane, which from linear algebra, has the notation null$(\nabla_{\mathbf{u}} g(\mathbf{p},\mathbf{u}^*))$ and now the condition changes such that the vector $\mathbf{u}^*$ must be orthogonal to the hyper-plane. The Euclidean distance from the origin in u-space to $(\mathbf{u})^*$ is given the symbol β and two examples are shown in Fig. 7.

Then for the ith limit-state function, the probability of non-conformance is found via the one-dimensional standard normal cumulative distribution function Φ and evaluated as

$$P(F_i) = \Phi(-\beta_i). \tag{22}$$

Further, the intersection probability of failure regions is important for accurate calculations in Eq. (19). For example, the intersection probability any two failure regions, say for hyper-plane LSSs i and j, is evaluated as

$$\begin{aligned} P(F_i \cap F_j) &= \Phi_2(-\beta_i, -\beta_j, \rho_{i,j}) \\ &= \int_{-\infty}^{-\beta_i}\int_{-\infty}^{-\beta_j} \frac{1}{2\pi\sqrt{1-\rho_{i,j}^2}} \exp\left(-\frac{u_1^2 - 2\rho_{i,j}u_1u_2 + u_2^2}{2(1-\rho_{i,j}^2)}\right) \mathrm{d}u_1\,\mathrm{d}u_2, \end{aligned} \tag{23}$$

where Φ_2 is the bivariate, cumulative, normal distribution function. The term $\rho_{i,j}$ indicates a sort of positional correlation coefficient (i.e. it ranges from -1 to $+1$) between two approximating LSSs, and is expressed as

$$\rho_{i,j} = \frac{\mathbf{u}_i^* \cdot \mathbf{u}_j^*}{||\mathbf{u}_i^*||_2 ||\mathbf{u}_j^*||_2}, \tag{24}$$

where $\mathbf{u}_i^*$ indicates the vector to the MLFP of the ith limit-state function. Numerical algorithms for evaluating the bi-normal cumulative function to accuracy 10^{-10} are given in Ref. [15].

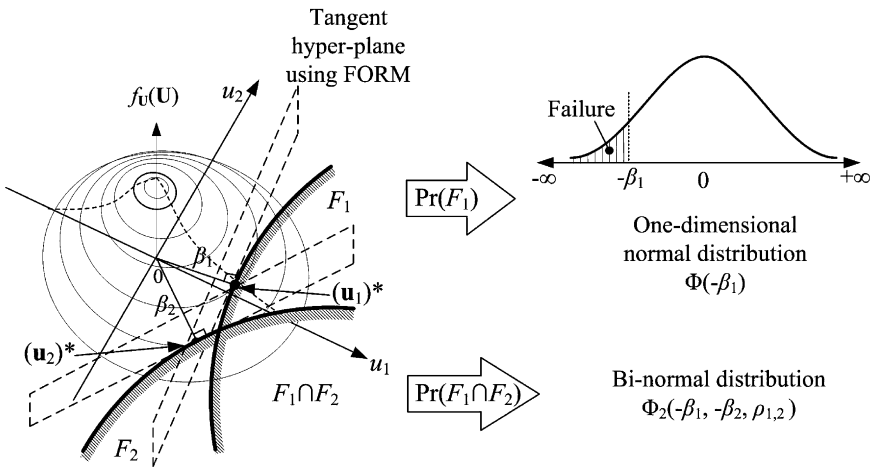

Fig. 7. Probability evaluation using FORM.

The system probability of non-conformance according to Eq. (19), and using the above FORM notation with second-order union probabilities, can be approximated as

$$P(F(\mathbf{p})) \cong \sum_{i=1}^{n} \Phi(-\beta_i(\mathbf{p})) - \sum_{i=2}^{n} \sum_{j=1}^{j<i} \Phi_2(-\beta_i(\mathbf{p}), -\beta_j(\mathbf{p}), \rho_{i,j}(\mathbf{p})). \tag{25}$$

The design problem for n limit-state functions is posed as a constrained optimization problem as follows:

$$\text{Min } P(F(\mathbf{p})) \tag{26}$$

subject to the constraints:

$$g_i(\mathbf{p}, \mathbf{u}) = 0 \quad \text{for } i = 1, 2, \ldots, n,$$

$$\mathbf{u}_i \cdot \text{null}(\nabla_{\mathbf{u}} g_i(\mathbf{p}, \mathbf{u})) = 0 \quad \text{for } i = 1, 2, \ldots, n,$$

$$\mathbf{p}_L \leqslant \mathbf{p} \leqslant \mathbf{p}_U,$$

where $\mathbf{p}_L$ and $\mathbf{p}_U$ are the lower and upper bounds, respectively, on the design parameters $\mathbf{p}$.

4. Absorber design example

4.1. Optimal probabilistic design

The proposed probabilistic design approach is now applied to the design of a vibration absorber for a steel box girder footbridge [10–12]. The footbridge is simplified to a lumped-parameter, mass-stiffner, system as shown in Fig. 1. The mass of the footbridge m_1 and the stiffness k_1 are independent random variables with lognormal distributions. The respective means are $\mu_1 = 17{,}500\,\text{kg}$ and $\mu_2 = 3.0\,\text{M N/m}$ and the respective standard deviations are set at $\sigma_1 = 10\mu_1/300\,\text{kg}$ and $\sigma_2 = 10\mu_2/300\,\text{M N/m}$. The **u**–**v** transformations are

$$v_i = \exp\left(\log\left(\frac{\mu_i^2}{\sqrt{\mu_i^2 + \sigma_i^2}}\right) + \log\left(\frac{\sigma_i^2}{\mu_i^2} + 1\right) u_i\right), \quad i = 1, 2. \tag{27}$$

At this time we let the design parameter vector be deterministic and thus $\mathbf{p} = [m_2, k_2, c_2]$ with lower and upper levels respectively $10 \leqslant m_2 \leqslant 1750\,\text{kg}$, $100 \leqslant k_2 \leqslant 10^6\,\text{N/m}$ and $10 \leqslant c_2 \leqslant 2000\,\text{N s/m}$. The sinusoidal loading has a constant amplitude of $P_0 = 0.48\,\text{kN}$ with a range of excitation frequencies given as $1 \leqslant \omega \leqslant 3w_2\,\text{rad/s}$. For purposes of comparison herein, we set $z_0 = 20$, although in general, the upper critical normalized amplitude of the main mass z_0 is set according to safety and/or comfort considerations.

The three sampled performance measures in **v**-space come from Eq. (14) and have the form $z_i(\mathbf{p},\mathbf{v})$. For example, for the critical frequency w_2, we have from Eq. (15)

$$z_2(\mathbf{p}, \mathbf{v}) = v_2 \left(\frac{c_2^2\left(\frac{v_2}{v_1}\right) + \left(k_2 - m_2\left(\frac{v_2}{v_1}\right)\right)^2}{c_2^2\left(\frac{v_2}{v_1}\right)\left(v_2 - v_1\left(\frac{v_2}{v_1}\right) - m_2\left(\frac{v_2}{v_1}\right)\right)^2 + \left(k_2 m_2\left(\frac{v_2}{v_1}\right) - \left(v_2 - v_1\left(\frac{v_2}{v_1}\right)\right)\left(k_2 - m_2\left(\frac{v_2}{v_1}\right)\right)\right)^2} \right)^{1/2}. \tag{28}$$

When we substitute the **u**–**v** transformations from Eq. (27) into Eq. (28), we get the performance measures $z_i(\mathbf{p},\mathbf{u})$. We now write the three limit-state functions as

$$g_i(\mathbf{p}, \mathbf{u}) = z_0 - z_i(\mathbf{p}, \mathbf{u}), \quad i = 1, 2, 3. \tag{29}$$

The combined probability of non-conformance, following the template in Eq. (16), is simply

$$P(F(\mathbf{p})) = P((g_1(\mathbf{p}, \mathbf{u}) < 0) \cup (g_2(\mathbf{p}, \mathbf{u}) < 0) \cup (g_3(\mathbf{p}, \mathbf{u}) < 0)). \tag{30}$$

For a FORM implementation of Eq. (30), we follow Eq. (25) to get

$$P(F(\mathbf{p})) = \sum_{i=1}^{3} \Phi(-\beta_i(\mathbf{p})) - \sum_{i=2}^{3} \sum_{j=1}^{j<i} \Phi_2(-\beta_i(\mathbf{p}), -\beta_j(\mathbf{p}), \rho_{i,j}(\mathbf{p})). \tag{31}$$

The parameters in the vibration absorber are found via the constrained optimization problem

$$\text{Min } P(F(\mathbf{p}) \tag{32}$$

subject to the constraints:

$$g_i(\mathbf{p},\mathbf{u}) = 0 \quad \text{for } i = 1,2,3,$$

$$\mathbf{u}_i \cdot \text{null}(\nabla_{\mathbf{u}} g_i(\mathbf{p},\mathbf{u})) = 0 \quad \text{for } i = 1,2,3.$$

$$-10 \leqslant m_2 \leqslant 1750\,\text{kg},$$

$$100 \leqslant k_2 \leqslant 10^6\,\text{N/m},$$

$$10 \leqslant c_2 \leqslant 2000\,\text{N s/m}.$$

The solution to the optimization problem in Eq. (32) is iterative and requires initial conditions. For convenience, we use the set of values in $\mathbf{p}_D$. The design obtained through solving Eq. (32) is $\mathbf{p}_P = [m_2,k_2,c_2] = [569.47\,\text{kg}, 88{,}400\,\text{N/m}, 2000\,\text{N s/m}]$ and the design gives $P(F(\mathbf{p}_P)) = 2.3 \times 10^{-10}$. The new design has increased the mass ratio to about 3.25% and increased the stiffness and damping in the vibration absorber considerably. Indeed the damping parameter c_2 has reached its upper bound. In order to see the significance of this design, consider the frequency responses for $a_n(\mathbf{p}_P,\mathbf{v}_{\#i},\omega)$. For the same 5000 samples of the mass and stiffness pairs used in Fig. 4, the maximum and minimum normalized amplitudes, at each frequency, are shown in Fig. 8. All maximum amplitudes over the frequency range are far remote from the critical limit. This design shows a significant improvement when compared to the deterministic design results in Fig. 4.

4.2. Design comparisons

Suppose we assign normal distributions for the mass and stiffness, rather than lognormal, to agree with those in our referenced work so that now the **u**–**v** transformations have the form $v_i = \mu_i + \sigma_i \mu_i$. The design results are very similar to those with lognormal distributions with only the mass decreasing by 2 kg. The similarities in the lognormal and normal results are not surprising since for both mass and stiffness $\sigma_i \ll \mu_i$ for $i = 1, 2$. Thus, the design $\mathbf{p}_P$ is used henceforth for comparison purposes.

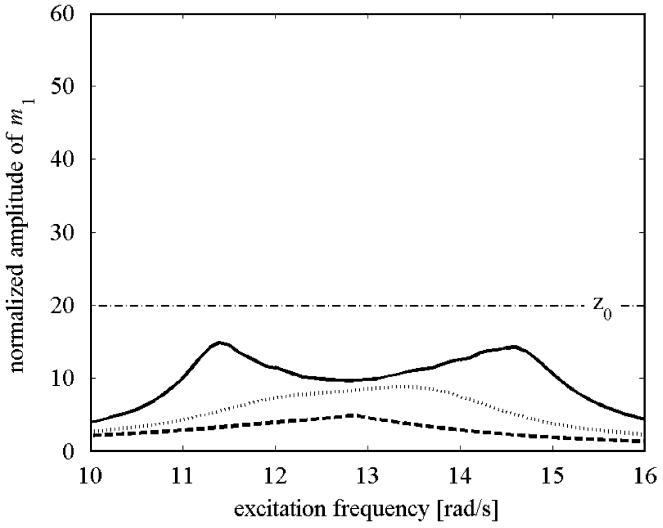

Fig. 8. Normalized amplitude of main mass at each frequency for new design $\mathbf{p}_P$ with m_1 and k_1 lognormally distributed: the dotted line is obtained with $\mathbf{v}_0$ and the line and dashed line represent the maximum and minimum amplitudes, respectively.

For a second, more representative comparison of the new design, the probabilistic design results presented in Ref. [10] are used. Therein the various designs are listed according to the weighting factor α used in the objective function shown in Eq. (1). Specifically, $\alpha = 0$, gives "Robust Design-1" and $\alpha = 1$ gives "Robust Design-11". Although the authors in Ref. [10] selected "Robust Design-6" as the most robust design, we have selected "Robust Design-11" where $\mathbf{p}_M = [m_2, k_2, c_2] = [510.93\,\text{kg},\ 84592\,\text{N/m},\ 2000\,\text{N s/m}]$ since our investigations show that this design provides the best competition for our approach. For example, with the critical limit $z_0 = 20$, we get $P(F(\mathbf{p}_M)) = 6 \times 10^{-7}$.

LSSs provide a simple graphical means of comparing designs. The LSSs are actually lines when there are only two design variables (i.e. V_1 and V_2) in the limit-state functions. Further, as shown in Fig. 9, all limit-state lines are practically linear, which suggests FORM probability estimations are quite accurate. Plots of the limit-state lines (with $\mathbf{p}$ specified) are obtained from implicit solutions of $g(u_1, u_2) = 0$. For comparison purposes, the limit-state lines from the three designs $\mathbf{p}_D$, $\mathbf{p}_M$ and $\mathbf{p}_P$ are shown in Fig. 9(a)–(c) respectively.

It should be noted that the limit-state line $g_2 = 0$ is actually an oval: this is not unexpected because of the high nonlinearity of the limit-state functions. Fortunately $g_2 = 0$ presents two, nearly parallel, lines that effectively straddle the origin. In many cases this may present a problem because only one MLFP per LSS is used. However, here it is not a problem, since on respective sides of the origin $\beta_2 \gg \beta_1$ and $\beta_2 \gg \beta_3$ for all three designs, and thus the non-conformance region $g_2 < 0$ is essentially contained in either $g_1 < 0$ or $g_3 < 0$ and any probability contribution is removed by intersection calculations. Also of interest are the relations $\beta_3 \ll \beta_2$ and $\beta_1 \ll \beta_2$ that tell us that the normalized amplitude is much more likely to exceed z_0 at frequencies w_1 and w_3 than at w_2.

In general, the farther a limit-state line is from the origin (and the larger β), the smaller the non-conformance region and hence the smaller the respective probability of non-conformance. Thus, when we use relative magnitudes of the indices β_1, β_2 and β_3, to compare designs $\mathbf{p}_D$, $\mathbf{p}_M$ and $\mathbf{p}_P$ it is clear graphically that $P(F(\mathbf{p}_P))$ and $P(F(\mathbf{p}_M)) << P(F(\mathbf{p}_D))$ and the two probabilistic designs are more robust. Finally, let us compare the two probabilistic designs $\mathbf{p}_M$ and $\mathbf{p}_P$. We see for $\mathbf{p}_M$ in Fig. 9(b) that $\beta_3 \gg \beta_1$ which suggests that this design is more likely to be non-conforming at w_1. However, for design $\mathbf{p}_P$ in Fig. 9(c), we see a more balanced design, although still $\beta_3 > \beta_1$, which suggests that the likelihood of non-conformance is not that different at either w_1 or w_3.

A more common graphical comparison uses plots of the mean and standard deviation of A_n over the frequency range. Good approximations of these measures for small variances in the design variables are written as follows [10]:

$$\mu(A_n) \approx A_n(\mu(V_1), \mu(V_2), \omega) \tag{33}$$

and

$$\sigma^2(A_n) \approx \left(\frac{\partial A_n(V_1, V_2, \omega)}{\partial V_1}\right)^2_{\mu(\mathbf{V})} \sigma^2(V_1) + \left(\frac{\partial A_n(V_1, V_2, \omega)}{\partial V_2}\right)^2_{\mu(\mathbf{V})} \sigma^2(V_2). \tag{34}$$

In Fig. 10 are plots of the mean and standard deviation using the three designs $\mathbf{p}_D$, $\mathbf{p}_M$ and $\mathbf{p}_P$ over the excitation frequency range.

It is clear that the proposed probabilistic approach effectively reduces both the mean and standard deviation of the normalized amplitude under the excitation force over a wide range of frequencies. Indeed, the absorber design $\mathbf{p}_P$ provides considerable improvement when compared with the deterministic design $\mathbf{p}_D$ over all frequencies. When compared with $\mathbf{p}_M$, design $\mathbf{p}_P$ shows generally a 10% improvement, especially around w_1 and w_2, although the results around w_3 are about 5% poorer.

5. Additional analyses

5.1. Relative motion of absorber mass

An important factor that has not been considered so far is the relative motion of the absorber mass with respect to the main mass. This measure is important since the displacement must not violate either

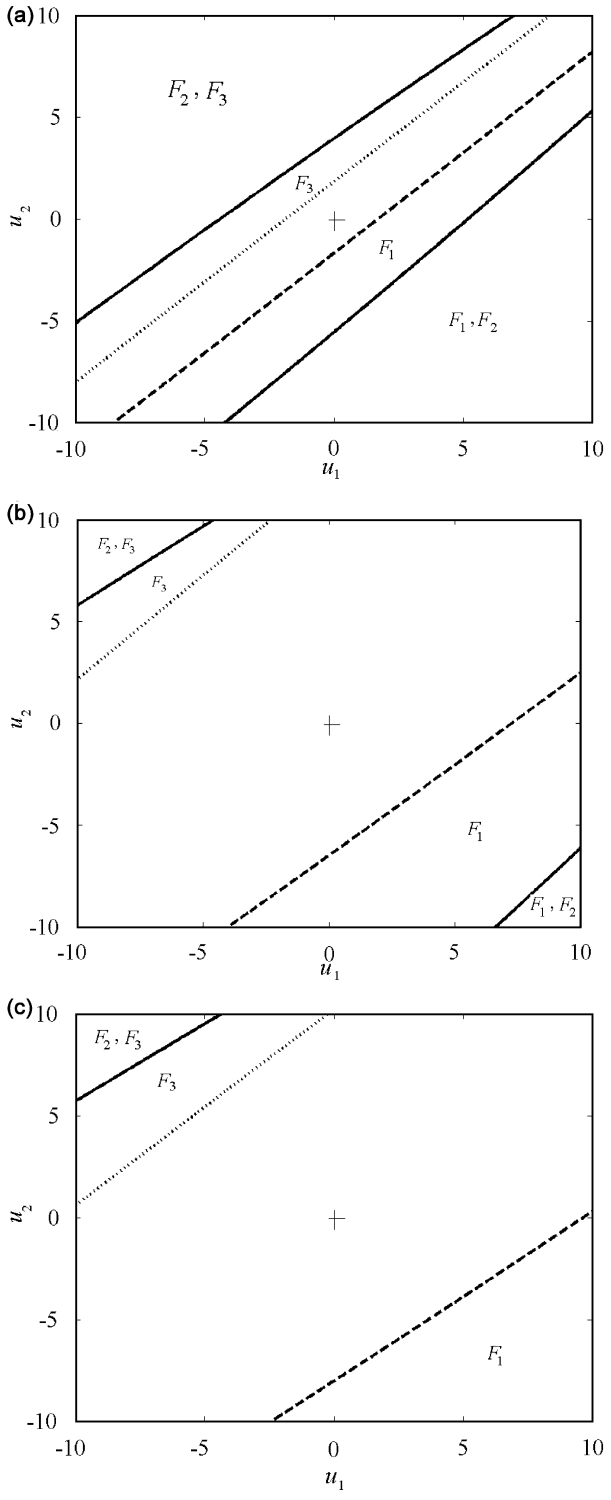

Fig. 9. Three limit-state surfaces $g_1 = 0$ (dashed line), $g_2 = 0$ (line), and $g_3 = 0$ (dotted line) where $F_1 = \{\mathbf{u} \in R^2 | g_1(\mathbf{p},\mathbf{u}) < 0\}$, $F_2 = \{\mathbf{u} \in R^2 | g_2(\mathbf{p},\mathbf{u}) < 0\}$, $F_3 = \{\mathbf{u} \in R^2 | g_3(\mathbf{p},\mathbf{u}) < 0\}$ for the three designs: (a) $\mathbf{p}_D$, (b) $\mathbf{p}_M$ and (c) $\mathbf{p}_P$.

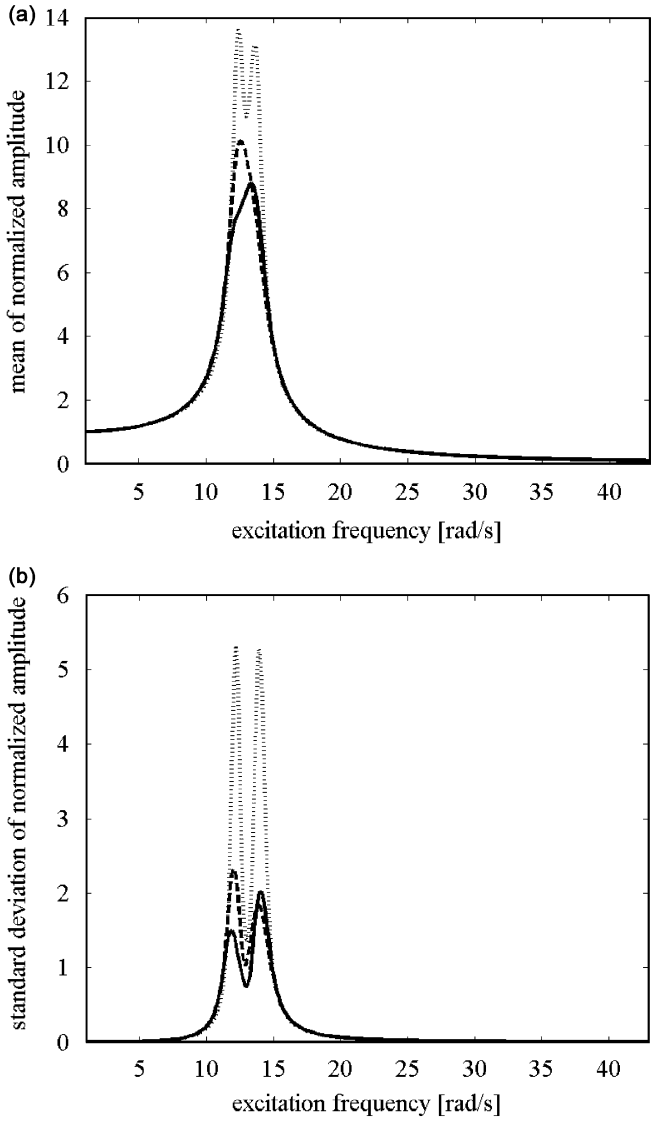

Fig. 10. Normalized amplitude A_n for designs $\mathbf{p}_D$ (dotted line), $\mathbf{p}_M$ (dashed line), and $\mathbf{p}_P$ (line) with (a) mean values and (b) standard deviation.

the compressed or extended physical limits of either the damper c_2 or the stiffener k_2. The relative motion is obtained as $(|x_2|-|x_1|)$ using Eqs. (4) and (5). The two probabilistic designs $\mathbf{p}_M$ and $\mathbf{p}_P$ are compared using the respective means and standard deviation that are calculated by adapting Eqs. (33) and (34). Plots are shown in Fig. 11(a) and (b). The proposed design $\mathbf{p}_P$ when compared with design $\mathbf{p}_M$ provides in general both a lower mean and a standard deviation over a wide range of excitation frequencies (except near w_3).

5.2. Uncertain parameters in the absorber subsystem

Let us consider uncertainty, not only in the main system, but in the vibration absorber subsystem as well. The proposed methodology is easily extended. Now, the mass m_2, stiffness k_2 and damping c_2 become random variables V_3, V_4 and V_5, respectively and so $\mathbf{V} = [V_1, V_2, V_3, V_4, V_5]$. The normalized amplitude has the

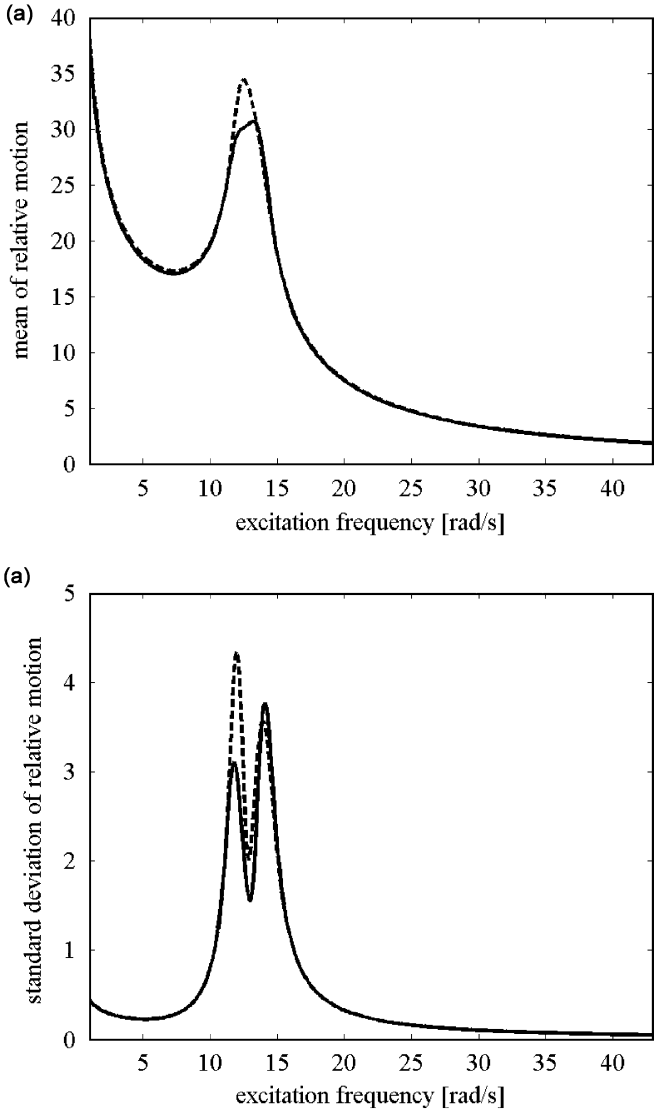

Fig. 11. Relative motion of m_2: (a) mean, and (b) standard deviation for designs $\mathbf{p}_M$ (dashed line) and $\mathbf{p}_P$ (line).

functional form

$$A_n = a_n(\mathbf{V}, \omega). \tag{35}$$

The distributions for V_3, V_4 and V_5 are chosen as lognormal and independent and their **u**–**v** transformations follow Eq. (27) where $\sigma_i = 10\mu_i/300$ for $i = 1,2\ldots5$.

The sampled performance measures are of the form $z_i(\mathbf{v})$. For example for z_2, with reference to Eqs. (15) and (28), we have

$$z_2(\mathbf{v}) = v_2\left(\frac{v_5^2\left(\frac{v_2}{v_1}\right) + \left(v_4 - v_3\left(\frac{v_2}{v_1}\right)\right)^2}{v_5^2\left(\frac{v_2}{v_1}\right)\left(v_2 - v_1\left(\frac{v_2}{v_1}\right) - v_3\left(\frac{v_2}{v_1}\right)\right)^2 + \left(v_4 v_3\left(\frac{v_2}{v_1}\right) - \left(v_2 - v_1\left(\frac{v_2}{v_1}\right)\right)\left(v_4 - v_3\left(\frac{v_2}{v_1}\right)\right)\right)^2}\right)^{1/2}. \tag{36}$$

when we substitute the **u**–**v** space transformations from Eq. (27) with $i = 1,2\ldots5$, we are left with the variables $\mathbf{p} = [\mu_3,\mu_4,\mu_5]$ and $\mathbf{u} = [u_1,u_2,u_3,u_4,u_5]$ to give the performance measures $z_i(\mathbf{p},\mathbf{u})$. The three limit-state functions, although quite different in make-up from those in Section 4, have the same symbolic form

$$g_i(\mathbf{p},\mathbf{u}) = z_0 - z_i(\mathbf{p},\mathbf{u}), \quad i = 1,2,3. \tag{37}$$

The optimization problem is an extension of Eq. (32) with m_2, k_2 and c_2 replaced by μ_3, μ_4 and μ_5. The solution of Eq. (32) provides the design parameter vector $\mathbf{p}_A = [571\,\text{kg},\ 87{,}914\,\text{N/m},\ 2000\,\text{N s/m}]$ and these results are not that different from $\mathbf{p}_P$. However we get $P(F(\mathbf{p}_A)) = 3.4\times10^{-6}$ and this is three orders of magnitude greater than $P(F(\mathbf{p}_P))$. Since there are now five design variables, it is not possible to visualize the LSSs graphically since they are four-dimensional (i.e. $n-1$).

5.3. Error analyses

In order to see how well $P(F(\mathbf{p}))$ represents the probability of non-conformance of the system over the entire frequency range, let us develop the true system probability of non-conformance. For this, we invoke Monte-Carlo simulation (MCS) and generate samples of **V** denoted as $[\mathbf{v}_{\#1}],[\mathbf{v}_{\#2}],\ldots,[\mathbf{v}_{\#N}]$ for $N = 10{,}000$. Then for each sample we check for non-conformance at a sequence of closely spaced frequencies (e.g. 0.1 rad/s) across the spectrum. Specifically, for the ith sample we evaluate $\text{sign}(a_n(\mathbf{p},\mathbf{v}_{\#I},\omega_k)-z_0)$ for $k = 1,2\ldots M$, at which $\omega_1 = 1$, $\omega_2 = 1.1,\ldots$ $\omega_M = 3w_2\,\text{rad/s}$. A positive sign at any ω_k indicates the sampled system has failed. Suppose there are B failed sampled systems, then we let the true system probability of non-conformance be $P(\text{MCS}(\mathbf{p})) = B/N$.

Further, lets us continually reduce the critical limit z_0 and then compare (a) designs $\mathbf{p}_D$, $\mathbf{p}_M$, $\mathbf{p}_P$ for normal distributions, and (b) designs $\mathbf{p}_D$, $\mathbf{p}_P$, $\mathbf{p}_A$ for lognormal distributions in terms of both $P(F(\mathbf{p}))$ and $P(\text{MCS}(\mathbf{p}))$. The results are shown in Tables 1 and 2 respectively.

The results show that the error between $P(F)$ and the true system probability of non-conformance $P(\text{MCS})$ increases as we reduce the critical limit z_0 from 20 to 11. This is not surprising since the normalized amplitudes at the critical frequencies are not the worst-case values over the frequency spectrum. This situation is shown in Fig. 3. Nevertheless, the proposed design $\mathbf{p}_P$ is always more robust than previous designs $\mathbf{p}_D$ and $\mathbf{p}_M$.

Table 1
$P(F(\mathbf{p}))$ and $P(\text{MCS}(\mathbf{p}))$ for $\mathbf{p} = \mathbf{p}_D$, $\mathbf{p}_M$, $\mathbf{p}_P$ according to z_0 for normally distributed m_1 and k_1

z_0	$\mathbf{p}_D$		$\mathbf{p}_M$		$\mathbf{p}_P$	
	$P(F)$	$P(\text{MCS})$	$P(F)$	$P(\text{MCS})$	$P(F)$	$P(\text{MCS})$
20	2.1×10^{-1}	3.0×10^{-1}	6.0×10^{-7}	2.0×10^{-4}	3.0×10^{-10}	0.0
17	4.3×10^{-1}	5.7×10^{-1}	2.2×10^{-5}	1.9×10^{-3}	2.9×10^{-8}	0.0
15	6.7×10^{-1}	8.6×10^{-1}	2.4×10^{-4}	1.6×10^{-2}	1.0×10^{-6}	1.0×10^{-4}
13	1.0	1.0	2.6×10^{-3}	1.0×10^{-1}	6.8×10^{-5}	3.9×10^{-3}
11	1.0	1.0	5.1×10^{-2}	5.2×10^{-1}	7.1×10^{-3}	1.1×10^{-1}

Table 2
$P(F(\mathbf{p}))$ and $P(\text{MCS}(\mathbf{p}))$ for $\mathbf{p} = \mathbf{p}_D$, $\mathbf{p}_P$, $\mathbf{p}_A$ according to z_0 for lognormally distributed m_1 and k_1

z_0	$\mathbf{p}_D$		$\mathbf{p}_P$		$\mathbf{p}_A$	
	$P(F)$	$P(\text{MCS})$	$P(F)$	$P(\text{MCS})$	$P(F)$	$P(\text{MCS})$
20	2.1×10^{-1}	3.1×10^{-1}	2.3×10^{-10}	0.0	3.4×10^{-6}	1.0×10^{-4}
17	4.3×10^{-1}	5.7×10^{-1}	2.7×10^{-8}	0.0	6.5×10^{-5}	1.3×10^{-3}
15	6.7×10^{-1}	8.6×10^{-1}	1.1×10^{-6}	0.0	6.3×10^{-4}	7.0×10^{-3}
13	9.9×10^{-1}	1.0	7.6×10^{-5}	5.6×10^{-3}	6.2×10^{-3}	5.2×10^{-2}
11	1.0	1.0	7.9×10^{-3}	1.0×10^{-1}	7.9×10^{-2}	2.7×10^{-1}

6. Conclusions

In this paper is presented a new probabilistic approach to produce a robust design when the resonance frequencies of a dynamic system are uncertain due to component variation. Herein lognormal distributions have been selected for design purposes while normal distributions have been assigned to help with comparisons to previous research (other distributions are possible and do not change the methodology). The forced vibration of a 2-dof system is examined and ways to minimize dynamic amplitude and its variation over a wide range of excitation frequencies are developed. In an attempt to manage the amplitude over the entire frequency range, three critical frequencies have been designated as surrogates for the frequency range. The key to the approach is the introduction, in a rational manner, of maximum critical amplitude. This leads to limit-state functions at each of the three critical frequencies that link respective amplitudes and the single critical limit. Each limit-state function provides a non-conformance region and the probability of the union of all three non-conformance regions provides a single, non-subjective, measure that is intended to represent the system probability of non-conformance. Constrained, gradient-based, nonlinear optimization methods have been invoked to allocate the design parameters to minimize the objective function. Studies using a range of values of the critical amplitude limit (i.e. $11 < z_0 < 20$) showed that improvements offered by the new approach are invariant to the value of the critical amplitude limit. However, the probability of non-conformance obtained in the course of the design may be quite different from the true system probability of non-conformance. More work is needed to close this difference.

The results of the proposed design method have been compared with those from (a) a deterministic design and (b) a second-moment probabilistic design. Further, the measures used to compare the three designs were (a) the probability of non-conformance measure, (b) the mean and standard deviation of amplitude over the frequency range, and, (c) the relative displacement of the absorber mass to the main mass. In all three of the comparisons, the new approach was overall superior.

The number of design variables and the number of performance measures can be expanded and still the single non-conformance probability objective can be applied. Herein, we increased the number of random design variables from two to five by letting the vibration absorber have uncertainty. Comparative results were obtained. Further, suppose we wish to include the relative motion of the absorber mass with respect to upper and lower critical lengths or the strength of the absorber stiffness with respect to an ultimate strength. These new performance measures can be described in terms of limit-state functions to augment those from the three amplitudes. The method may be extended to (a) vibration problems with more than 2-dof, and, integrated design, whereby means and tolerances are simultaneously found, provided a suitable cost function is available to effectively allocate the tolerances. For cases when the critical frequencies are not explicit functions of the design variables, it may be necessary to be more flexible and select a judicious number of deterministic frequencies to represent the overall frequency spectrum. More investigation in this area needs to be done.

References

[1] M.S. Phadke, *Quality Engineering using Robust Design*, Prentice-Hall, Englewood Cliffs, NJ, 1989.
[2] J.C. Zhang, M.A. Styblinski, *Yield and Variability Optimization of Integrated Circuits*, Kluwer Academic Publishers, Boston, 1995.
[3] R. Spence, S.R. Soin, *Tolerance Design of Electronic Circuits*, Imperial College Press, London, 1997.
[4] R. Seshadri, G.J. Savage, Integrated robust design with probability of conformance metric, *International Journal of Materials and Product Technology* 17 (2002) 319–337.
[5] G.J. Savage, R. Seshadri, Minimizing cost of multiple response systems by probabilistic robust design, *Quality Engineering* 16 (2003) 67–74.
[6] G.J. Savage, D. Tong, S.M. Carr, Optimal mean and tolerance allocation using conformance-based design, *Quality and Reliability Engineering International* 22 (2006) 445–472.
[7] K. Yang, B. El-Haik, *Design for Six Sigma: A Roadmap for Product Development*, McGraw-Hill, New York, 2003.
[8] K. Seki, K. Ishill, M. Esterman, Robust design for dynamic performance: optical pick-up example, *Proceedings of the 1997 ASME Design Engineering Technical Conference and Design Automation Conference, Sacrament*, CA, Paper No. 97-DETC/DAC3978, 1997.
[9] K.H. Hwang, K.W. Lee, G.J. Park, Robust optimization of an automobile rearview mirror for vibration reduction, *Structural and Multidisciplinary Optimization* 21 (2001) 300–308.
[10] C. Zang, M.I. Friswell, J.E. Mottershead, A review of robust optimal design and its application in dynamics, *Computers and Structures* 83 (2005) 315–326.

[11] D.J. Inman, *Engineering Vibration*, Prentice-Hall, Englewood Cliffs, NJ, 1996.
[12] J.W. Smith, *Vibration of Structures: Applications in Civil Engineering Design*, Chapman & Hall, London, 1998.
[13] R.E. Melcher, *Structural Reliability Analysis and Prediction*, Wiley, Chichester, 1987.
[14] M. Rosenblatt, Remarks on a multivariate transformation, *Annual of Mathematical Statistics* 23 (1952) 470–472.
[15] A. Genz, Numerical computation of rectangular bivariate and trivariate normal and t probabilities, *Statistics and Computing* 14 (2004) 151–160.